

Graphene oxide-composited chitosan scaffold contributes to functional recovery of injured spinal cord in rats

<https://doi.org/10.4103/1673-5374.306095>

Date of submission: March 9, 2020

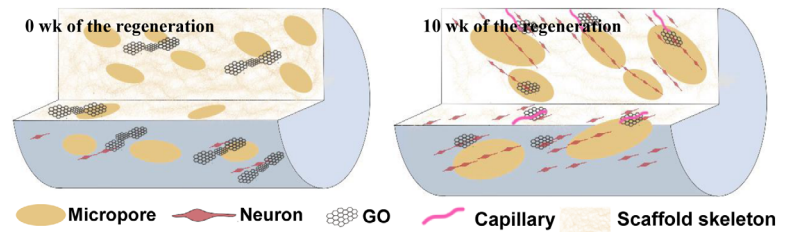
Date of decision: June 22, 2020

Date of acceptance: November 20, 2020

Date of web publication: January 25, 2021

Bing Yang^{1, #}, Pang-Bo Wang^{2, #}, Ning Mu², Kang Ma², Shi Wang², Chuan-Yan Yang², Zhong-Bing Huang^{1, *}, Ying Lai², Hua Feng², Guang-Fu Yin¹, Tu-Nan Chen^{2, *}, Chen-Shi Hu¹

Graphical Abstract *Neuronal migration into the chitosan-graphene oxide (GO) scaffold*



Abstract

The study illustrates that graphene oxide nanosheets can endow materials with continuous electrical conductivity for up to 4 weeks. Conductive nerve scaffolds can bridge a sciatic nerve injury and guide the growth of neurons; however, whether the scaffolds can be used for the repair of spinal cord nerve injuries remains to be explored. In this study, a conductive graphene oxide composited chitosan scaffold was fabricated by genipin crosslinking and lyophilization. The prepared chitosan-graphene oxide scaffold presented a porous structure with an inner diameter of 18–87 μm , and a conductivity that reached 2.83 mS/cm because of good distribution of the graphene oxide nanosheets, which could be degraded by peroxidase. The chitosan-graphene oxide scaffold was transplanted into a T9 total resected rat spinal cord. The results show that the chitosan-graphene oxide scaffold induces nerve cells to grow into the pores between chitosan molecular chains, inducing angiogenesis in regenerated tissue, and promote neuron migration and neural tissue regeneration in the pores of the scaffold, thereby promoting the repair of damaged nerve tissue. The behavioral and electrophysiological results suggest that the chitosan-graphene oxide scaffold could significantly restore the neurological function of rats. Moreover, the functional recovery of rats treated with chitosan-graphene oxide scaffold was better than that treated with chitosan scaffold. The results show that graphene oxide could have a positive role in the recovery of neurological function after spinal cord injury by promoting the degradation of the scaffold, adhesion, and migration of nerve cells to the scaffold. This study was approved by the Ethics Committee of Animal Research at the First Affiliated Hospital of Third Military Medical University (Army Medical University) (approval No. AMUWEC20191327) on August 30, 2019.

Key Words: angiogenesis; chitosan; electrical conduction; graphene oxide; regeneration; repair; scaffold; spinal cord injury

Chinese Library Classification No. R452; R744; R318.08

Introduction

Traumatic spinal cord injury (SCI) occurs when an external physical effect abruptly damages the spinal cord. Nearly half a million of people suffer from SCI each year (Lazaridis and Andrews, 2014). SCI causes catastrophic physical and mental trauma to patients, and introduces a heavy economic burden to society and victimized families because of long-term hospitalization, poor rehabilitation outcome, and excessive dependence on care (Soufiany et al., 2018; Wang et al., 2019a; Ray, 2020). However, to date, there is no effective clinical treatment of SCI (Alves-Sampaio et al., 2016; Huang

and Zoubi, 2018).

Therapeutic strategies that bridge spinal cord cystic cavities and replace lost tissue have gradually been of focus (Huang et al., 2018; Li et al., 2019). Ideally, nerve scaffolds, a tissue engineering product, could provide support for neural regeneration and axon extension to avoid transplant rejection. Various biocompatible materials, such as collagen, hyaluronic acid, chitosan (CS) and polylactic-co-glycolic acid, have been used for bridging spinal cord defects (Shi et al., 2014; Wen et al., 2016; Zheng et al., 2017). CS is a novel material in the field of spinal nerve regeneration because of its excellent

¹College of Biomedical Engineering, Sichuan University, Chengdu, Sichuan Province, China; ²Department of Neurosurgery, Southwest Hospital, Third Military Medical University (Army Medical University), Chongqing, China

*Correspondence to: Zhong-Bing Huang, PhD, zbhuang@scu.edu.cn; Tu-Nan Chen, PhD, ctn@tmmu.edu.cn.

<https://orcid.org/0000-0002-3834-471X> (Zhong-Bing Huang); <https://orcid.org/0000-0003-0460-5632> (Tu-Nan Chen)

#Both authors contributed equally to this work.

Funding: This work was supported by the National Key Research and Development Program of China, No. 2018YFC1106800 (to ZBH and GFY), Sichuan Science and Technology Project of China, No. 2018JY0535 (to ZBH), Talents Training Program of Army Medical University of China, No. 2019MPCRC021/SWH2018QNWQ-05 (to TNC) and Research on Key Technologies of Photoelectromagnetic Acoustic Intensity Brain of China, No. AWS16J025 (to HF).

How to cite this article: Yang B, Wang PB, Mu N, Ma K, Wang S, Yang CY, Huang ZB, Lai Y, Feng H, Yin GF, Chen TN, Hu CS (2021) Graphene oxide-composited chitosan scaffold contributes to functional recovery of injured spinal cord in rats. *Neural Regen Res* 16(9):1829-1835.

biocompatibility, biodegradability, and bacteriostatic properties (Jayakumar et al., 2007; Xu et al., 2019; Yan et al., 2019). The degradation product of CS, chitooligosaccharide, could promote cell proliferation and prevent apoptosis especially for Schwann cells (Zhao et al., 2017), indicating that CS could be a promising candidate for repair of SCI (Chen et al., 2011; Zhang et al., 2016).

Endogenous bioelectric signals play an important role in maintaining neuronal function, neurite growth, and tissue regeneration (Benfenati et al., 2013; Zhou et al., 2018; Chen et al., 2019). A biomaterial-based therapy that could bridge cystic cavities and mimic the electrical conduction properties of the spinal cord is beneficial for SCI repair (Zhou et al., 2018). This inspires us to design conductive materials with good electrical conductivity and softness in accordance with spinal cord tissue to promote axonal regeneration. In recent years, graphene-derived materials have displayed great potential for neural tissue engineering because they could serve as a platform to support and direct neural growth (Das et al., 2017). Graphene oxide (GO), a major derivative, possesses the properties of graphene (e.g., mechanical ductility, electrical conductivity, and stiffness), as well as better biocompatibility and higher hydrophilicity than pristine graphene (Hong et al., 2012; Tan et al., 2013). GO can accelerate the migration, proliferation, and myelination of Schwann cells and differentiation of PC12 cells (Wang et al., 2019b). *In vivo* studies also revealed the capacity of GO/reduced GO (rGO) to permit neurogenesis, immunomodulatory, and angiogenic responses by regulating the intracellular expression of reactive oxygen and nitrogen species, and the AKT-nitric oxide synthase-vascular endothelial growth factor signaling pathway (Defterali et al., 2016; López-Dolado et al., 2016; Qian et al., 2018b; Domínguez-Bajo et al., 2019). The main differences between GO and rGO are better biocompatibility, degradation behavior and lower electrical conductivity of GO compared with rGO because of better transmission of electrical signal for mediating cell behavior via its π bonds. However, previous *in vivo* studies investigated the ability of GO for SCI with hemisection. The toxicity of a scaffold fabricated by pure GO is important because an overdose of a graphene-based material may induce organ necrosis (Ema et al., 2017). Therefore, CS is an ideal skeleton material for a scaffold and the addition of GO nanosheets could introduce conductivity to the scaffold to promote nerve regeneration. In this work, GO-composited CS (CS-GO) scaffolds were prepared by genipin-crosslinking and lyophilization. The CS-GO scaffolds were evaluated by neural cell tests and *in vivo* bridge treatment in the cross-section of a SCI.

Materials and Methods

Fabrication of porous CS-GO scaffolds

A CS solution with a concentration of 2% (w/v) was prepared by dissolving CS powder in 1% (v/v) acetic acid under gentle shaking. GO with a concentration of 0.2% (w/v) was dispersed in deionized water for 5 hours of ultrasonic shaking. The preparation of the CS-GO composite scaffolds was according to the following method, as illustrated in **Additional Figure 1**. First, the GO suspension, with a weight proportion of 1% CS, was ultrasonically mixed with the CS solution, and the pure CS solution was used as control. CS molecule chains, with abundant amino groups, have strong electrostatic attraction with the carboxyl groups from GO (Compton and Nguyen, 2010), as shown in **Additional Figure 1A**. These solutions were mixed with genipin solution (1% w/v) at ratio of 1:100 of CS solution, respectively, and blended for 2 hours at 37°C, which was the best ratio to decrease swelling and retain the topology of the scaffold according to the previous report (Lau et al., 2018). The amino groups of CS could be linked by genipin, thus improving the mechanical strength of the scaffold (**Additional Figure 1B**). After degassing in vacuum, two blends were injected into a 3 × 30 mm silicone tube and

a 48-well cell culture plate, respectively. The sample solution was then frozen at -20°C and lyophilized at -50°C for 12 hours to produce porous scaffolds of CS or GO-CS. CS and GO-CS films were fabricated by liquid casting, respectively, to evaluate their electrical conductivity. The physical and chemical properties were evaluated in **Additional File 1**.

Cytotoxicity test

The cytotoxicity of the CS and CS-GO scaffolds were evaluated using a 3-(4,5-dimethylthiazol-2-yl)-2,5-diphenyltetrazolium bromide (MTT) assay by culturing PC12 cells in a 48-well plate. The PC12 cells were obtained from Shanghai Institute of Bio-chemistry and Biology (Shanghai, China). The plates and scaffolds were sterilized with 75% ethanol for 30 minutes. Subsequently, all scaffolds were washed with phosphate-buffered saline (PBS) three times and exposed to ultraviolet light for 12 hours. PC12 cell suspension (0.5 mL) with cell density of 5×10^4 cells/mL was added to each well and cultivated for 1, 2, and 3 days. Every 24 hours, the wells were rinsed with PBS and refreshed with 0.5 mL of Dulbecco's modified Eagle's medium. Subsequently, cells were incubated in 0.5 mL of MTT solution (5 mg/mL) at 37°C for 4 hours. The supernatant of each well was removed and 0.4 mL of dimethyl sulfoxide was added to each well and shaken for 10 minutes to dissolve the intracellular formazan crystal. Finally, 200 μ L of the supernatant from each well was transferred to a 96-well culture plate and the absorbance was measured at a wavelength of 480 nm using a microplate reader (VERSA max, Molecular Devices, Sunnyvale, CA, USA).

Establishment of the SCI transection model and scaffold transplantation

All animal operations were approved by the Ethics Committee of Animal Research at the First Affiliated Hospital of Third Military Medical University (Army Medical University; No. AMUWEC20191327) on August 30, 2019. All Sprague-Dawley rats were provided by the Animal Center of the Third Military Medical University (Army Medical University), Chongqing, China (license No. SCXK (Yu) 2017002). After 1 week of adaptation, clean, adult, 6–8 weeks old, female Sprague-Dawley rats with a weight of 200 ± 20 g were used as model animals. The rats were intraperitoneally injected with 2 mg/mL ethyl carbamate (0.1 mL/10 g) anesthesia, and then fixed to the operating table (Cai et al., 2019). After the skin and subcutaneous muscles were cut open, the lamina of the thoracic vertebrae T8–10 were exposed. The spinal cord was exposed and approximately 2 mm of the spinal cord tissue at the T9 level was completely removed under an operating microscope. Rats immediately showed a tail wagging reflex, hind limb and torso retraction and flutter, and subsequent paralysis of the hind limbs, suggesting the successful fabrication of the SCI model (Boato et al., 2010). SCI rats were randomly divided into three groups: the Control group treated with 200 μ L of PBS injection ($n = 5$), the CS group ($n = 5$), and the CS-GO group ($n = 5$). After sufficient hemostasis, the CS and CS-GO scaffolds (length of 2 mm and diameter of 3.5 mm) were implanted into the spinal cord gap and the muscle and skin of these rats were sutured with 4-0 nylon sutures. Each rat received a daily intramuscular injection of penicillin and levofloxacin for seven consecutive days to prevent infection, and the bladder was emptied every 12 hours until the rats recovered autonomic urination (Yuan et al., 2015).

Basso, Beattie, and Bresnahan locomotor rating scale evaluation

Assessment of the locomotion function of the rat hind limb was performed with the Basso, Beattie, and Bresnahan (BBB) scale (Basso et al., 1995) 1 day after surgery, and was repeated once a week through 10 weeks. Briefly, rats were allowed to move freely on a circular platform with a diameter of 2 m, and were observed for at least 5 minutes by two observers

who were blinded to the research. A score ranging from 0 to 21 points was assessed based on conditions such as joint activities, coordination of fore and hind limbs, and trunk and tail positions. Six rats (two for each group) from each group were randomly selected for the assessment at each time.

Electrophysiological recording

Four mice were randomly chosen from each group and anesthetized with 1% pentobarbital sodium (25 mg/kg intraperitoneal injection) to record the somatosensory evoked potentials (SSEP) elicited by transcranial electrical stimulation (Xia et al., 2019; All et al., 2020). The needle electrodes were inserted subcutaneously with the tip touching the skull. The reference electrode was placed between the eyes. The recording electrode was placed between the ears. The hindlimbs of mice were exposed to enable insertion of stimulating electrodes into the gastrocnemius muscles. A ground electrode was placed subcutaneously at the base of the tail. The gastrocnemius muscle was electrically stimulated using a stimulator (Keypoint, Medtronic, Minneapolis, MN, USA). A single pulse of stimulation (0.8 mA, 10 ms, 2 Hz) was performed via stimulation of needle electrodes (DSN1620, Medtronic). Each rat received 100 consecutive positive monophasic current pulses until the waveform was stable. The first trough of the signal curve from the beginning of the stimulation appeared as P40. The gap time between troughs was latency and the first peak that appeared was called N50. In addition, the second trough that appeared was P60. The gap between the lowest trough and crest was the amplitude. This operation was performed at least twice per rat.

Histological analysis

Rats were sacrificed with 2 mg/mL ethyl carbamate (0.1 mL/10 g) through intraperitoneal injection 10 weeks after the transplantation. Subsequently, rats were perfused rapidly with approximately 200 mL iced saline per rat. The rats were fixed by perfusing with 4% paraformaldehyde. 0.5 cm of the spinal cord sections in the rostral and caudal direction with respect to the injury center were removed, dehydrated, embedded, and cryo-sectioned into slices with a thickness of 5 μ m. These slices were then stained with hematoxylin and eosin. Immunofluorescence staining was then performed according to Mengchu's protocol (Cui et al., 2019). Briefly, the sections were sequentially permeabilized in 0.3% Triton X-100 (Sigma, St. Louis, MO, USA) at room temperature for 15 minutes after antigen retrieval with citric acid. The sections were blocked in 5% goat serum at 37°C for 2 hours, and then incubated with primary antibodies overnight at 4°C, which included goat anti-microtubule-associated protein-2 polyclonal antibody (Cat# ab5392; 1:1000; Abcam, Boston, MA, USA) for regenerated axons and goat anti-choline acetyltransferase (ChAT) polyclonal antibody (Cat# AB144P; 1:500; R&D, Minneapolis, MN, USA) for cholinergic motor neurons and premotor interneurons. The sections were rinsed in 0.1 M of PBS three times for 5 minutes each, and then incubated with the corresponding secondary antibodies for 2 hours at room temperature: Alexa Fluor 488-conjugated goat anti-chicken IgG (Cat# ab150169; 1:200; Abcam) and Alexa Fluor 568-conjugated donkey anti-goat IgG (Cat# ab150131; 1:50; Abcam). Immunofluorescence images were obtained by confocal microscopy (LSM800; ZEISS, Oberkochen, Germany) and a Virtual Slide Microscope (VS120; Olympus LifeScience, Tokyo, Japan).

Statistical analysis

All statistical analyses were performed using IBM SPSS Statistics 20 (IBM Corp., Armonk, NY, USA). Data are expressed as mean \pm standard error. The two groups were analyzed using a two-tailed Student's *t*-test. A repeated-measures analysis of variance was adopted to analyze the data from the same

sample at different time points for the behavior assessment and latency of SSEP. The Student's *t*-test was used for single comparison. *P* < 0.05 and 0.01 were considered statistically significant.

Results

Morphology and structure of the CS-GO scaffolds

The porous structure of the scaffold can support tissue ingrowth, neuron migration, and metabolic waste discharge. Image of the internal microstructure of the fabricated CS-GO scaffold with a 3 mm diameter is shown in **Figure 1A**, indicating that the pores were irregular and randomly distributed. The inner diameter of these pores was 18–87 μ m (average 37 μ m, as shown in **Figure 1B**), suggesting that the pore size was suitable for cell migration (Liu et al., 2016). Additionally, the pore surface of the CS-GO scaffold with many fine bumps was rough (**Additional Figure 2A**), while the pore surface of the CS scaffold was smoother (**Additional Figure 2B**), indicating the presence of GO sheet on the surface of the micropores and good distribution of GO nanosheets in the CS matrix.

Figure 1C displays the Fourier-transform infrared spectroscopy spectra of the CS and CS-GO scaffolds. The peaks of the amide I band of C=O stretching at 1645 cm^{-1} , amide II band of C-N stretching at 1564 cm^{-1} , and amide III band of N-H deformation at 1409 cm^{-1} in the two patterns indicate that the amino groups of CS were crosslinked by genipin, forming amide groups. The Raman spectra of the two scaffolds in **Figure 1D** show that there was a distinct D-band at 1350 cm^{-1} , G-band at 1605 cm^{-1} , and 2D-band at 2657 cm^{-1} in the pattern of CS-GO, suggesting the existence of GO; the small peak at 2900 cm^{-1} is attributed to the second-order model (D and G bands), further suggesting the existence of GO in the CS-GO sample. The atomic force microscope morphology image in **Figure 1E** showed that there were fine and dense nano-bulges on the pore surface of the GO-CS scaffold that originated from the even distribution of GO nanosheets on the surface of the micropores. The height of these nano-bulges was \sim 30 nm, and the bulge height did not significantly impede cell growth. However, there were a few nano-bulges on the pore surface of the CS scaffold in the atomic force microscope image in **Additional Figure 2C**, and the height of these bulges was less than 10 nm. These few bulges might originate from clusters of CS molecule-chains on the pore surface.

As shown in **Additional Figure 2D**, the addition of GO significantly improved the stress (from 190 MPa to 500 MPa) and elasticity (from 17% to 32%) of the scaffold because of the electrostatic interaction between the amino groups of CS and the carboxyl groups of GO (**Additional Figure 1**), which is important for the adhesion and ingrowth of neurons. Furthermore, the addition of less GO at 1% could increase the electrical conductivity from \sim 0.05 mS/cm (dry CS film) to \sim 1.19 mS/cm (dry CS-GO film, **Additional Figure 3D**) because of the even distribution of GO sheets on/in the surface/inside of film. The conductivity increased to \sim 2.83 mS/cm after immersion in PBS because the micropores of the CS-GO film were filled with ionic aqueous liquid. This result encouraged multi-stage *in vivo* bioelectrical signals transmission in the GO-added matrix because the conductivity of the CS-GO film nearly reached the reported range of the spinal cord tissue conductivity of \sim 10 mS/cm (Holsheimer, 1998). Although the conductivity of the CS-GO film decreased to \sim 0.54 mS/cm because of detachment of some of the GO from the CS matrix after 14 days of immersion, CS-GO can still transfer electrical signals to a certain extent.

Sufficient attention should be given to the potential toxicity of graphene-based materials. Clinical application of GO is dependent on its degradation. The *in vivo* environment has abundant active oxygen and peroxidase from neutrophil granulocytes. Some studies have shown the biodegradation

of graphene-based materials by peroxidase in the presence of H_2O_2 (Kotchey et al., 2011; Kurapati et al., 2015). **Additional Figure 3A** showed the larger undegraded GO sheets; however, the GO sheets in **Additional Figure 3B** were smaller because of oxidation by horseradish peroxidase and H_2O_2 . As shown in **Additional Figure 3C**, the mean size of the GO decreased from ~360 nm to 245.6 nm after 24 hours of degradation by horseradish peroxidase, suggesting that biodegradability of GO from the peroxidase of neutrophil granulocytes could occur (Kotchey et al., 2011).

Cytotoxicity of the CS-GO scaffold

The cytotoxicity of the prepared scaffolds was analyzed by MTT assay. The cell viability of the PC12 cells on the CS-GO scaffold was significantly less than those on the CS in the first 2 days (**Figure 1F**). However, the cell viability on the CS-GO scaffold increased over time, and there was no difference between the two samples on day 3, which was attributed to the formation of protein corona near GO leading to the enhanced cell viability. This result suggests the biosafety of GO for the growth of neurocytes, corresponding to previous reports (López-Dolado et al., 2016; Domínguez-Bajo et al., 2019).

CS-GO scaffolds improve the functional recovery of SCI rats

After the excision of the rat spinal cord, different grafts were transplanted to the defect site through microsurgery (**Figure 2A**). As shown in **Figure 2B**, the BBB scores of all rats were close to 0 the first day after SCI, and subsequently recovered to different degrees over time, with all animals showing different degrees of functional recovery at 10 weeks. The locomotion recovery of the CS-GO group started seven weeks after SCI (**Figure 2B**), and the BBB score reached a level of 8–9 at 10 weeks, suggesting the CS-GO scaffold could significantly improve the functional recovery compared with the Control ($P < 0.01$) and CS groups ($P < 0.05$).

Furthermore, the SSEP of different groups was evaluated 10 weeks after SCI. The latent period (red line in **Figure 2C**) of the three groups showed a trend of “Control > CS > CS-GO”, and the amplitude showed a trend of “Control < CS < CS-GO” (**Figure 2E**). The quantitative results illustrate that the SSEP latency of the CS-GO group was significantly less than that of the Control and CS groups ($P < 0.05$; **Figure 2D**). Subsequently, all rats were sacrificed 10 weeks after SCI to evaluate the effect of the CS and CS-GO on tissue repair. The CS-GO scaffold was surrounded by regenerative neural tissue (**Figure 2F**). The diameters of the proximal stumps of three groups were same, indicating the proximal spinal tissue did not atrophy. However, compared with the Control group, the cauda equina in the distal stumps (**Figure 2F**) of the CS and CS-GO groups was not atrophied, indicating a protective function of the CS and CS-GO scaffolds in the spinal cord by allowing signal transmission between two injury sites.

CS-GO scaffolds reduce pathological damage in the spinal cord of SCI rats

Hematoxylin and eosin staining and immunohistochemistry were performed to assess tissue bridging and neuronal regeneration. In the Control group, tissue at the injury site was disordered and many cavities were observed (**Additional Figure 4A**). In the CS group, the lesion site was filled with materials and no tissue inside the CS scaffold was observed (**Additional Figure 4B**). However, in the CS-GO group, regularly organized tissue at the injury site was observed, and the regenerated tissue was arranged along the channels of the CS-GO scaffold (**Additional Figure 4C**), suggesting that the addition of GO nanosheets could induce neuron migration and tissue ingrowth, which is consistent with a previous report (Palejwala et al., 2016).

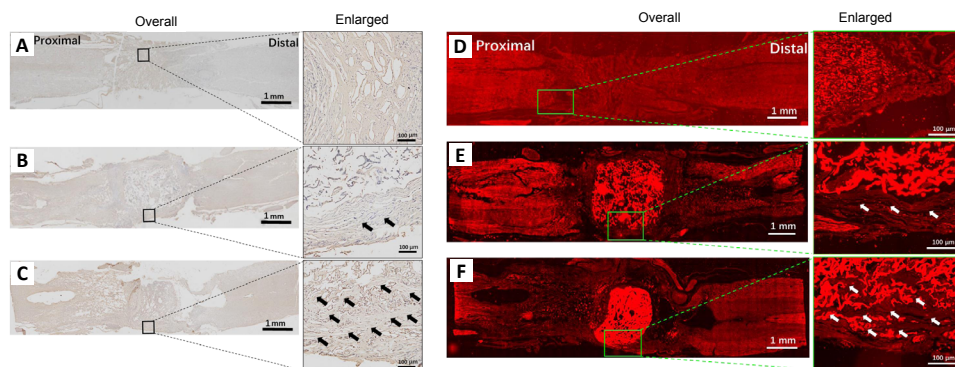
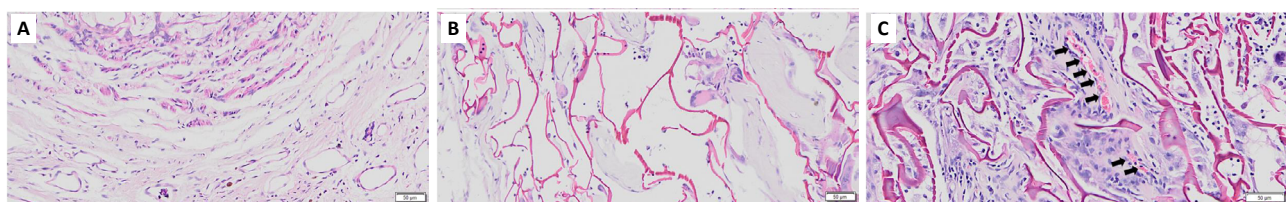
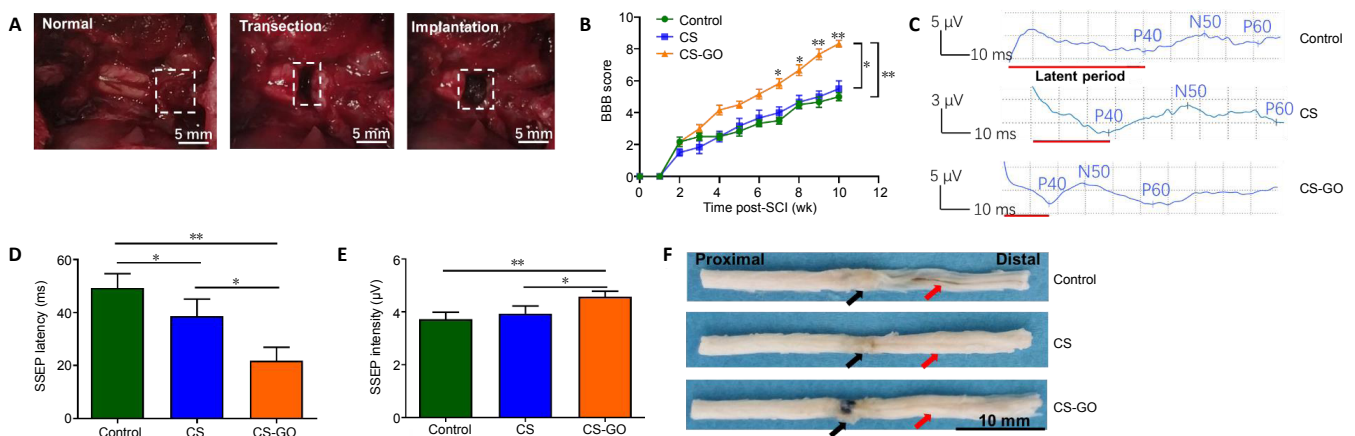
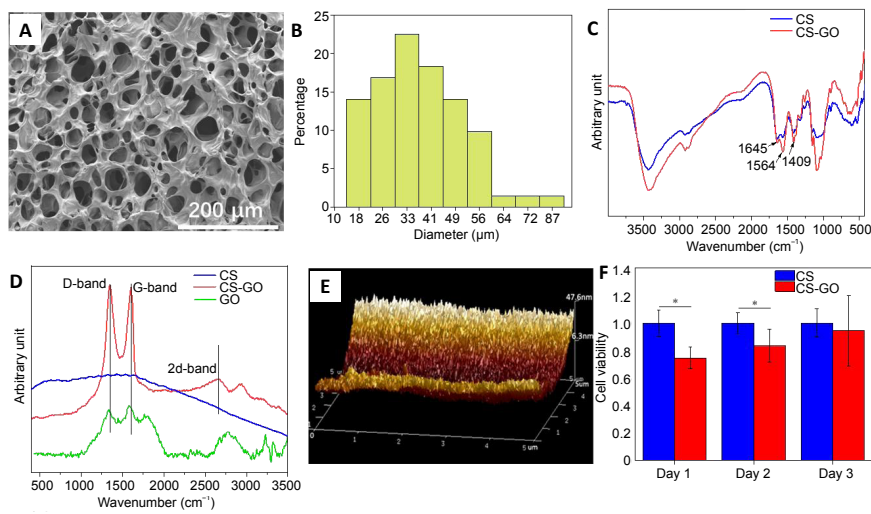
Compared with the CS scaffold, there are more cell nuclei in

the injury sites of the CS-GO scaffold, indicating that the GO addition enhanced the cyto-compatibility of the CS matrix, promoting neurocytes to grow into the larger pores of the CS-GO scaffold (**Figure 3**). The regenerated neuronal cells were growing inside the structure of the CS-GO scaffold. Compared with the Control and CS groups, the erythrocytes in the CS-GO scaffold (**Figure 3C**) indicate angiogenesis. It was reported that a bare GO scaffold could induce angiogenic responses in nerve repair (Mukherjee et al., 2015; López-Dolado et al., 2016), and further support axon regrowth and functional recovery after SCI. Capillaries provide necessary supplies and molecular mediators for new tissue growth, as well as mobilize endogenous progenitor cells that can drive neurogenesis at the center of the lesion site (Rauch et al., 2009). Thus, the addition of GO is important for angiogenesis, neurogenesis, and further functional recovery after SCI.

ChAT expression, which represents the cholinergic motor neurons and premotor interneurons, is associated with neurite outgrowth (Kumamaru et al., 2018) and represents nerve regeneration. As shown in **Figure 4A**, there were obvious broken tissue ends in the injury sites of the Control group. Some ChAT-positive neurons on the surface of the CS scaffold appeared (**Figure 4B**) and the extended axon did not migrate into the inner structure of the scaffold. More ChAT-positive neurons were observed on the surface of the GO-CS scaffold. However, ordered directional extension along the material structure inside the GO-CS scaffold also appeared (**Figure 4C**), indicating GO promoted neuronal migration and axon extension into the CS-GO scaffold (López-Dolado et al., 2016; Domínguez-Bajo et al., 2019).

The expression of microtubule-associated protein-2 is associated with regenerative axon. Different degrees of atrophy were observed in the Control and CS groups (**Additional Figure 5A and B**). The spinal cord of the Control group was atrophied and nearly disrupted (**Additional Figure 5A**) at the injury site. There was still a small amount of atrophy observed in **Additional Figure 5B**, although the atrophy in the CS group was less than that in the Control group. Regenerative neurons did not grow into the CS scaffold. Alternatively, there was no significant atrophy observed at the injury site of the CS-GO group, and a few regenerated neural fibers were observed (as indicated by arrows in **Additional Figure 5C**), suggesting the impact of GO in nerve regeneration.

The ChAT staining images showed similar results to immunohistochemistry. GO was previously demonstrated to promote the directional growth of axons (Zhou et al., 2018). As shown in **Figure 4D**, there was no neurite outgrowth in the Control group, and the size of the retained fibers of the degraded CS was larger than that of the degraded GO-CS (**Figure 4E and F**) because the addition of hydrophilic GO induced a stronger force between macromolecule chains, preventing swelling of CS-GO, leading to the smaller fiber size of CS-GO. However, both CS and CS-GO scaffolds were surrounded by regenerative neurites (**Figure 4E and F**), suggesting the supportive effect of the CS skeleton for nerve adhesion. The regenerative tissues were growing along the surface of the CS scaffold (**Figure 4E**). However, as shown in **Figure 4F**, the regenerative tissues grew along the surface of the CS-GO scaffold and directionally migrated into the inner pores, promoting the degradation of CS chains. These results were in accordance with a previous study (Domínguez-Bajo et al., 2019). The size distribution of these pores was evaluated based on the images of hematoxylin and eosin-stained sections of the regenerated tissue, and shown in **Additional Figure 6**. The size of the micropores in CS-GO increased to 30–160 μm , which was larger than the 18–87 μm of the implanted scaffold, suggesting that the *in vivo* environment resulted in degradation of the CS molecule chains and GO nanosheets during regeneration over 10 weeks. Moreover, the mean pore diameter of the CS-GO scaffold increased from ~37



mm before the implantation to ~79 μm after implantation, and the increase of 42 μm was smaller than the change of 52 μm for the CS scaffold (from 58 mm before implantation to ~110 μm after implantation), indicating that the polar linkage between the GO nanosheets and CS matrix slightly slowed the degradation of the CS molecule chains.

Discussion

GO can upregulate neural expression via its unique nanostructure (Qian et al., 2018a). It was reported that the addition of a low percentage of GO/rGO could promote neuronal migration into a porous scaffold, along with angiogenesis because of the π bond distribution on the surface of the GO sheet. As a result, the promotion mechanism of the CS-GO scaffold on the *in vivo* regeneration of SCI was proposed. There are many micropores in our prepared GO-CS scaffold and GO sheets were evenly distributed on the micropores surface, which promoted cell attachment of the neurons at an early stage after implantation because of the π - π interactions of the GO layer with aromatic amino acids in the cell membrane (Rajesh et al., 2009; Lee et al., 2011). After 10 weeks of repair, neuron attachment could induce regenerated tissues to directionally grow into those micropores, and the *in vivo* degradation of the GO nanosheets and CS matrix of the scaffold led to a thinner skeleton, which increased the size of micropores and reduced the size of the GO sheets. Alternatively, the angiogenic process can be induced by regulating the intracellular expression of reactive oxygen and nitrogen species from GO sheets (Mukherjee et al., 2015; Qian et al., 2018a). Regenerated capillaries could provide necessary nutrition for neuronal regeneration, further guiding the proliferation and migration of neurocytes. Finally, the conductivity of the CS-GO scaffold during regeneration also introduced better electrical signal delivery in the repair site to promote the migration/growth of neurocytes (Chen et al., 2019) and the functional recovery of the regenerated tissue.

A conductive CS-GO composite scaffold was fabricated by genipin-crosslinking. Genipin possesses more biocompatibility than other common crosslink agents (such as glutaraldehyde), and can promote the alignment and proliferation of neuronal cells (Lau et al., 2018). In addition, the porous structure of the scaffold was formed with lyophilization so that nutrients and metabolic waste were easily exchanged through the penetrated micropores. The electrical conductivity of the CS-GO scaffold reached ~2.83 mS/cm because of even distribution of the GO sheets in the scaffold, and these GO nanosheets could be biodegraded by peroxidase into the finer nanosheets. The results of the *in vivo* repair of SCI with total resection indicate that, the CS-GO scaffold could significantly induce functional recovery seven weeks after SCI. The addition of GO can induce angiogenesis and promote the directional growth of regenerated tissues into the larger micropores 10 weeks after SCI. These results indicate the potential of GO on the regeneration and functional recovery of SCI and nerve regeneration. A higher conductivity CS-GO scaffold may favor the regeneration of SCI, and the effect of electrical stimulation on spinal cord regeneration and its mechanism should be studied in future work.

Author contributions: Study design: ZBH and TNC; study conception: HF and GFY; scaffold preparation: BY and PBW; scaffold evaluation: CSH; animal experiment: PBW, NM, and KM; tissue analyses: SW, CYY, and YL; manuscript writing: BY and PBW. All authors approved the final version of the manuscript.

Conflicts of interest: The authors declare that they have no competing interests.

Financial support: This work was supported by the National Key Research and Development Program of China, No. 2018YFC1106800 (to ZBH and GFY), Sichuan Science and Technology Project of China, No. 2018JY0535 (to ZBH), Talents Training Program of Army Medical University of China,

No. 2019MPRC021/SWH2018QNWQ-05 (to TNC) and Research on Key Technologies of Photoelectromagnetic Acoustic Intensity Brain of China, No. AWS16J025 (to HF). The funding sources had no role in study conception and design, data analysis or interpretation, paper writing or deciding to submit this paper for publication.

Institutional review board statement: This study was approved by the Ethics Committee of Animal Research at the First Affiliated Hospital of Third Military Medical University (Army Medical University) (approval No. AMUWEC20191327) on August 30, 2019.

Copyright license agreement: The Copyright License Agreement has been signed by all authors before publication.

Data sharing statement: Datasets analyzed during the current study are available from the corresponding author on reasonable request.

Plagiarism check: Checked twice by iThenticate.

Peer review: Externally peer reviewed.

Open access statement: This is an open access journal, and articles are distributed under the terms of the Creative Commons Attribution-NonCommercial-ShareAlike 4.0 License, which allows others to remix, tweak, and build upon the work non-commercially, as long as appropriate credit is given and the new creations are licensed under the identical terms.

Additional files:

Additional file 1: The physical and chemical properties of CS-GO scaffolds.

Additional Figure 1: Schematic of preparation of CS-GO scaffold.

Additional Figure 2: Microstructure and mechanical strength of CS-GO and CS scaffold.

Additional Figure 3: Biodegradation of GO by horseradish peroxidase.

Additional Figure 4: Hematoxylin and eosin staining assessment on the longitudinal sections of the spinal cords of (A) control, (B) CS, (C) CS-GO groups.

Additional Figure 5: Immunofluorescence (MAP2) staining of the injured site of (A) control, (B) CS, (C) CS-GO groups.

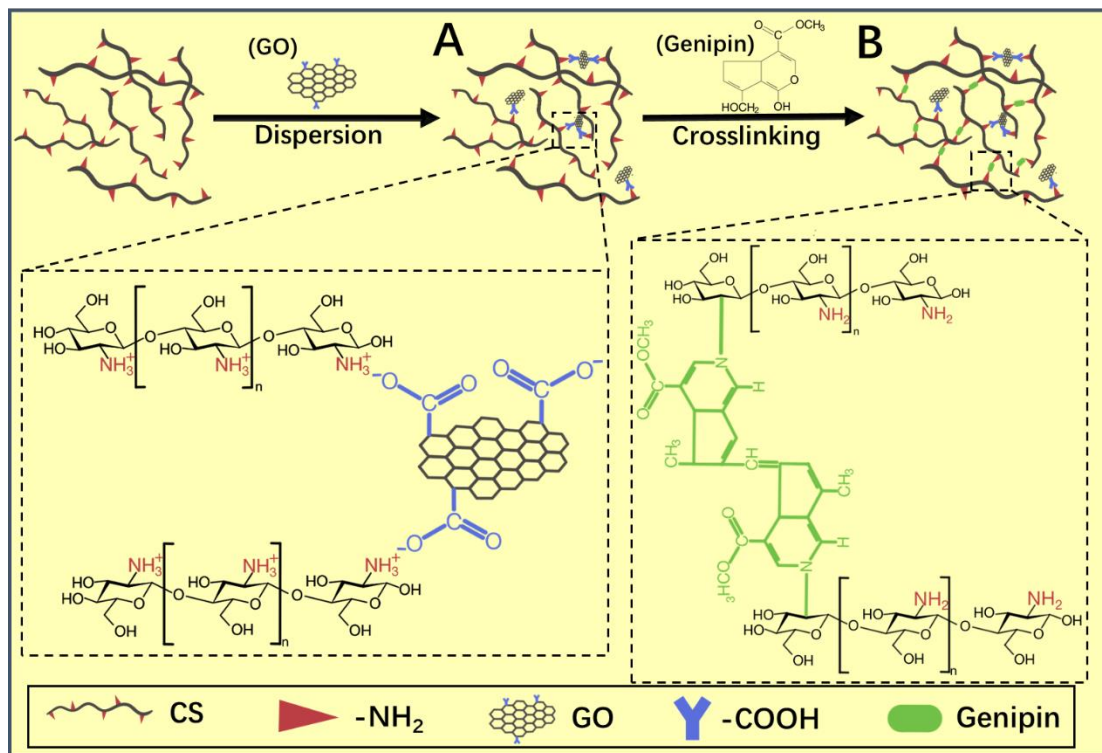
Additional Figure 6: The diameter distributions of the inner micropores of GO-CS and CS scaffolds implanted for 10 weeks, based on the images of hematoxylin and eosin-stained section of their regeneration tissue.

References

- All AH, Al Nashash H, Mir H, Luo S, Liu X (2020) Characterization of transection spinal cord injuries by monitoring somatosensory evoked potentials and motor behavior. *Brain Res Bull* 156:150-163.
- Alves-Sampaio A, Garcia-Rama C, Collazos-Castro JE (2016) Biofunctionalized PEDOT-coated microfibers for the treatment of spinal cord injury. *Biomaterials* 89:98-113.
- Basso DM, Beattie MS, Bresnahan JC (1995) A sensitive and reliable locomotor rating scale for open field testing in rats. *J Neurotrauma* 12:1-21.
- Benfenati V, Toffanin S, Bonetti S, Turatti G, Pistone A, Chiappalone M, Sagnella A, Stefani A, Generali G, Ruani G, Saguatti D, Zamboni R, Muccini M (2013) A transparent organic transistor structure for bidirectional stimulation and recording of primary neurons. *Nat Mater* 12:672-680.
- Boato F, Hendrix S, Huelsenbeck SC, Hofmann F, Grosse G, Djalali S, Klimaschewski L, Auer M, Just I, Ahnert-Hilger G, Hölting M (2010) C3 peptide enhances recovery from spinal cord injury by improved regenerative growth of descending fiber tracts. *J Cell Sci* 123:1652-1662.
- Cai Z, Gan Y, Bao C, Wu W, Wang X, Zhang Z, Zhou Q, Lin Q, Yang Y, Zhu L (2019) Photosensitive hydrogel creates favorable biological niches to promote spinal cord injury repair. *Adv Healthc Mater* 8:e1900013.
- Chen X, Liu C, Huang Z, Pu X, Shang L, Yin G, Xue C (2019) Preparation of carboxylic graphene oxide-composited polypyrrole conduits and their effect on sciatic nerve repair under electrical stimulation. *J Biomed Mater Res A* 107:2784-2795.
- Chen X, Yang Y, Yao J, Lin W, Li Y, Chen Y, Gao Y, Yang Y, Gu X, Wang X (2011) Bone marrow stromal cells-loaded chitosan conduits promote repair of complete transection injury in rat spinal cord. *J Mater Sci Mater Med* 22:2347-2356.
- Compton OC, Nguyen ST (2010) Graphene oxide, highly reduced graphene oxide, and graphene: versatile building blocks for carbon-based materials. *Small* 6:711-723.
- Cui M, Ge H, Zeng H, Yan H, Zhang L, Feng H, Chen Y (2019) Repetitive transcranial magnetic stimulation promotes neural stem cell proliferation and differentiation after intracerebral hemorrhage in mice. *Cell Transplant* 28:568-584.

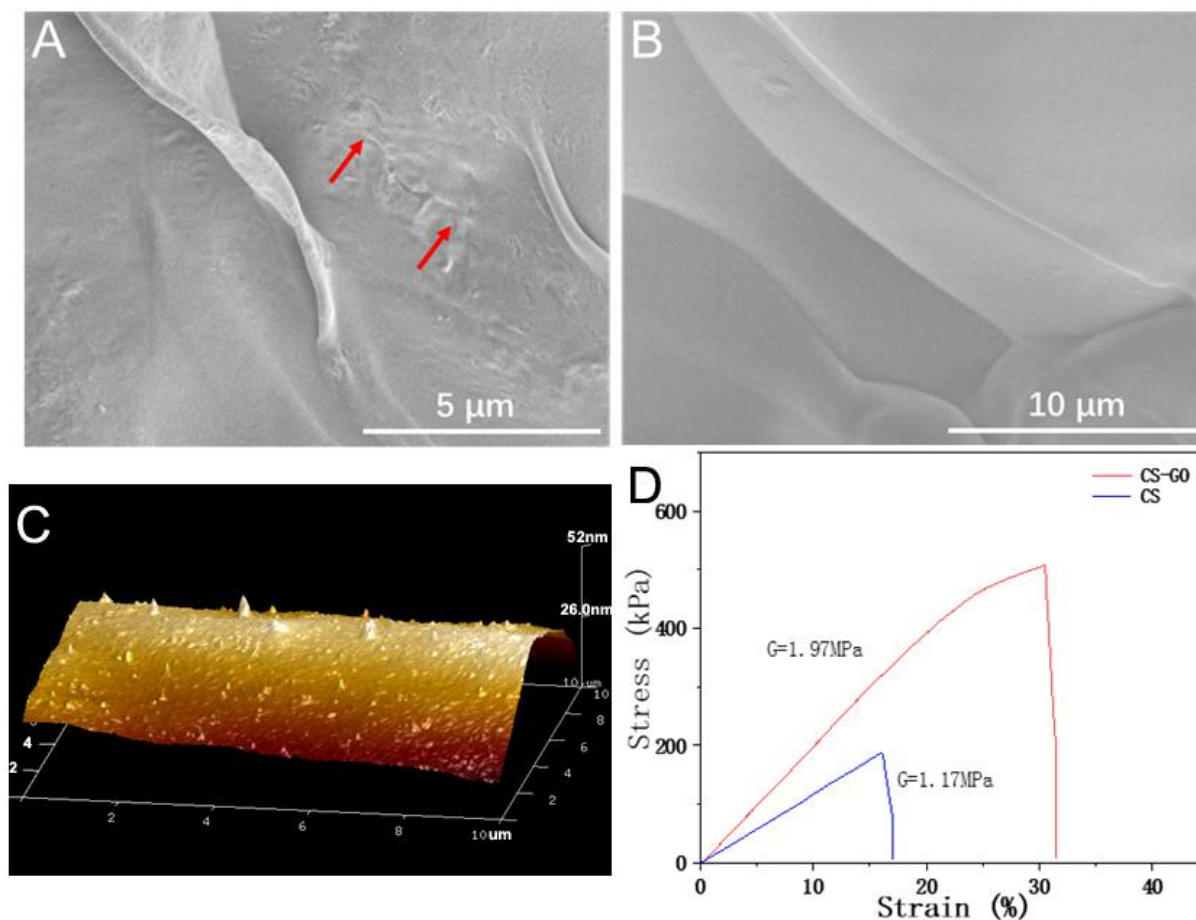
- Das SR, Uz M, Ding S, Lentner MT, Hondred JA, Cargill AA, Sakaguchi DS, Mallapragada S, Claussen JC (2017) Electrical differentiation of mesenchymal stem cells into Schwann-cell-like phenotypes using inkjet-printed graphene circuits. *Adv Healthc Mater* 6:1601087.
- Defterali Ç, Verdejo R, Peponi L, Martín ED, Martínez-Murillo R, López-Manchado M, Vicario-Abejón C (2016) Thermally reduced graphene is a permissive material for neurons and astrocytes and de novo neurogenesis in the adult olfactory bulb in vivo. *Biomaterials* 82:84-93.
- Domínguez-Bajo A, González-Mayorga A, Guerrero CR, Palomares FJ, García R, López-Dolado E, Serrano MC (2019) Myelinated axons and functional blood vessels populate mechanically compliant rGO foams in chronic cervical hemisectioned rats. *Biomaterials* 192:461-474.
- Ema M, Gamo M, Honda K (2017) A review of toxicity studies on graphene-based nanomaterials in laboratory animals. *Regul Toxicol Pharmacol* 85:7-24.
- Holsheimer J (1998) Computer modelling of spinal cord stimulation and its contribution to therapeutic efficacy. *Spinal Cord* 36:531-540.
- Hong BJ, Compton OC, An Z, Eryazici I, Nguyen ST (2012) Successful stabilization of graphene oxide in electrolyte solutions: enhancement of biofunctionalization and cellular uptake. *ACS Nano* 6:63-73.
- Huang H, Zoubi ZMA (2018) A brief introduction to the Special Issue on clinical treatment of spinal cord injury. *J Neurorestorol* 6:134-135.
- Huang H, Sharma HS, Chen L, Otom A, Al Zoubi ZM, Saberi H, Muresanu DF, He X (2018) Review of clinical neurorestorative strategies for spinal cord injury: Exploring history and latest progresses. *J Neurorestorol* 6:171-178.
- Jayakumar R, Nwe N, Tokura S, Tamura H (2007) Sulfated chitin and chitosan as novel biomaterials. *Int J Biol Macromol* 40:175-181.
- Kotchey GP, Allen BL, Vedala H, Yanamala N, Kapralov AA, Tyurina YY, Klein-Seetharaman J, Kagan VE, Star A (2011) The enzymatic oxidation of graphene oxide. *ACS Nano* 5:2098-2108.
- Kumamaru H, Kadoya K, Adler AF, Takashima Y, Graham L, Coppola G, Tuszyński MH (2018) Generation and post-injury integration of human spinal cord neural stem cells. *Nat Methods* 15:723-731.
- Kurapati R, Russier J, Squillaci MA, Treossi E, Ménard-Moyon C, Del Rio-Castillo AE, Vazquez E, Samorì P, Palermo V, Bianco A (2015) Dispersibility-dependent biodegradation of graphene oxide by myeloperoxidase. *Small* 11:3985-3994.
- Lau YT, Kwok LF, Tam KW, Chan YS, Shum DK, Shea GK (2018) Genipin-treated chitosan nanofibers as a novel scaffold for nerve guidance channel design. *Colloids Surf B Biointerfaces* 162:126-134.
- Lazaridis C, Andrews CM (2014) Traumatic spinal cord injury: learn from the brain!*. *Crit Care Med* 42:749-750.
- Lee WC, Lim CH, Shi H, Tang LA, Wang Y, Lim CT, Loh KP (2011) Origin of enhanced stem cell growth and differentiation on graphene and graphene oxide. *ACS Nano* 5:7334-7341.
- Li J, He L, Zhang Y (2019) Application of multishot diffusion tensor imaging in spinal cord tumors. *Brain Sci Adv* 5:59-64.
- Liu C, Kray J, Toomajian V, Chan C (2016) Schwann cells migration on patterned polydimethylsiloxane microgrooved surface. *Tissue Engineering Part C, Methods* 22:644-651.
- López-Dolado E, González-Mayorga A, Gutiérrez MC, Serrano MC (2016) Immunomodulatory and angiogenic responses induced by graphene oxide scaffolds in chronic spinal hemisectioned rats. *Biomaterials* 99:72-81.
- Mukherjee S, Sriram P, Barui AK, Nethi SK, Veeriah V, Chatterjee S, Suresh KI, Patra CR (2015) Graphene oxides show angiogenic properties. *Adv Healthc Mater* 4:1722-1732.
- Palejwala AH, Fridley JS, Mata JA, Samuel EL, Luerssen TG, Perlaky L, Kent TA, Tour JM, Jea A (2016) Biocompatibility of reduced graphene oxide nanoscaffolds following acute spinal cord injury in rats. *Surg Neurol Int* 7:75.
- Qian Y, Zhao X, Han Q, Chen W, Li H, Yuan W (2018a) An integrated multi-layer 3D-fabrication of PDA/RGD coated graphene loaded PCL nanoscaffold for peripheral nerve restoration. *Nat Commun* 9:323.
- Qian Y, Song J, Zhao X, Chen W, Ouyang Y, Yuan W, Fan C (2018b) 3D fabrication with integration molding of a graphene oxide/polycaprolactone nanoscaffold for neurite regeneration and angiogenesis. *Adv Sci (Weinh)* 5:1700499.
- Rajesh C, Majumder C, Mizuseki H, Kawazoe Y (2009) A theoretical study on the interaction of aromatic amino acids with graphene and single walled carbon nanotube. *J Chem Phys* 130:124911.
- Rauch MF, Hynes SR, Bertram J, Redmond A, Robinson R, Williams C, Xu H, Madri JA, Lavik EB (2009) Engineering angiogenesis following spinal cord injury: a coculture of neural progenitor and endothelial cells in a degradable polymer implant leads to an increase in vessel density and formation of the blood-spinal cord barrier. *Eur J Neurosci* 29:132-145.
- Ray SK (2020) Modulation of autophagy for neuroprotection and functional recovery in traumatic spinal cord injury. *Neural Regen Res* 15:1601-1612.
- Shi Q, Gao W, Han X, Zhu X, Sun J, Xie F, Hou X, Yang H, Dai J, Chen L (2014) Collagen scaffolds modified with collagen-binding bFGF promotes the neural regeneration in a rat hemisectioned spinal cord injury model. *Sci China Life Sci* 57:232-240.
- Soufiany I, Hijrat KA, Soufiany S, Chen L (2018) Mechanisms and major sites of distal catheter migration in ventriculoperitoneal shunting maneuvers: a review article. *Brain Sci Adv* 4:141-155.
- Tan X, Feng L, Zhang J, Yang K, Zhang S, Liu Z, Peng R (2013) Functionalization of graphene oxide generates a unique interface for selective serum protein interactions. *ACS Appl Mater Interfaces* 5:1370-1377.
- Wang C, Zhang L, Ndong JC, Hettinghouse A, Sun G, Chen C, Zhang C, Liu R, Liu CJ (2019a) Progranulin deficiency exacerbates spinal cord injury by promoting neuroinflammation and cell apoptosis in mice. *J Neuroinflammation* 16:238.
- Wang J, Cheng Y, Chen L, Zhu T, Ye K, Jia C, Wang H, Zhu M, Fan C, Mo X (2019b) In vitro and in vivo studies of electroactive reduced graphene oxide-modified nanofiber scaffolds for peripheral nerve regeneration. *Acta Biomater* 84:98-113.
- Wen Y, Yu S, Wu Y, Ju R, Wang H, Liu Y, Wang Y, Xu Q (2016) Spinal cord injury repair by implantation of structured hyaluronic acid scaffold with PLGA microspheres in the rat. *Cell Tissue Res* 364:17-28.
- Xia M, Chen W, Wang J, Yin Y, Guo C, Li C, Li M, Tang X, Jia Z, Hu R, Liu X, Feng H (2019) TRPA1 activation-induced myelin degradation plays a key role in motor dysfunction after intracerebral hemorrhage. *Front Mol Neurosci* 12:98.
- Xu Y, Huang Z, Pu X, Yin G, Zhang J (2019) Fabrication of chitosan/polypyrrole-coated poly(L-lactic acid)/polycaprolactone aligned fibre films for enhancement of neural cell compatibility and neurite growth. *Cell Prolif* 52:e12588.
- Yan F, Li M, Zhang HQ, Li GL, Hua Y, Shen Y, Ji XM, Wu CJ, An H, Ren M (2019) Collagen-chitosan scaffold impregnated with bone marrow mesenchymal stem cells for treatment of traumatic brain injury. *Neural Regen Res* 14:1780-1786.
- Yuan J, Zou M, Xiang X, Zhu H, Chu W, Liu W, Chen F, Lin J (2015) Curcumin improves neural function after spinal cord injury by the joint inhibition of the intracellular and extracellular components of glial scar. *J Surg Res* 195:235-245.
- Zhang J, Lu X, Feng G, Gu Z, Sun Y, Bao G, Xu G, Lu Y, Chen J, Xu L, Feng X, Cui Z (2016) Chitosan scaffolds induce human dental pulp stem cells to neural differentiation: potential roles for spinal cord injury therapy. *Cell Tissue Res* 366:129-142.
- Zhao Y, Wang Y, Gong J, Yang L, Niu C, Ni X, Wang Y, Peng S, Gu X, Sun C, Yang Y (2017) Chitosan degradation products facilitate peripheral nerve regeneration by improving macrophage-constructed microenvironments. *Biomaterials* 134:64-77.
- Zheng HB, Luo L, Chen L (2017) Tissue-engineered spinal cord construction by chitosan alginate scaffold and adipose-derived mesenchymal stem cells in the treatment of acute spinal cord injury. *Zhongguo Zuzhi Gongcheng Yanjiu* 21:4199-4204.
- Zhou L, Fan L, Yi X, Zhou Z, Liu C, Fu R, Dai C, Wang Z, Chen X, Yu P, Chen D, Tan G, Wang Q, Ning C (2018) Soft conducting polymer hydrogels cross-linked and doped by tannic acid for spinal cord injury repair. *ACS Nano* 12:10957-10967.

C-Editor: Zhao M; S-Editors: Yu J, Li CH; L-Editors: Cooper A, Wysong S, Qiu Y, Song LP; T-Editor: Jia Y



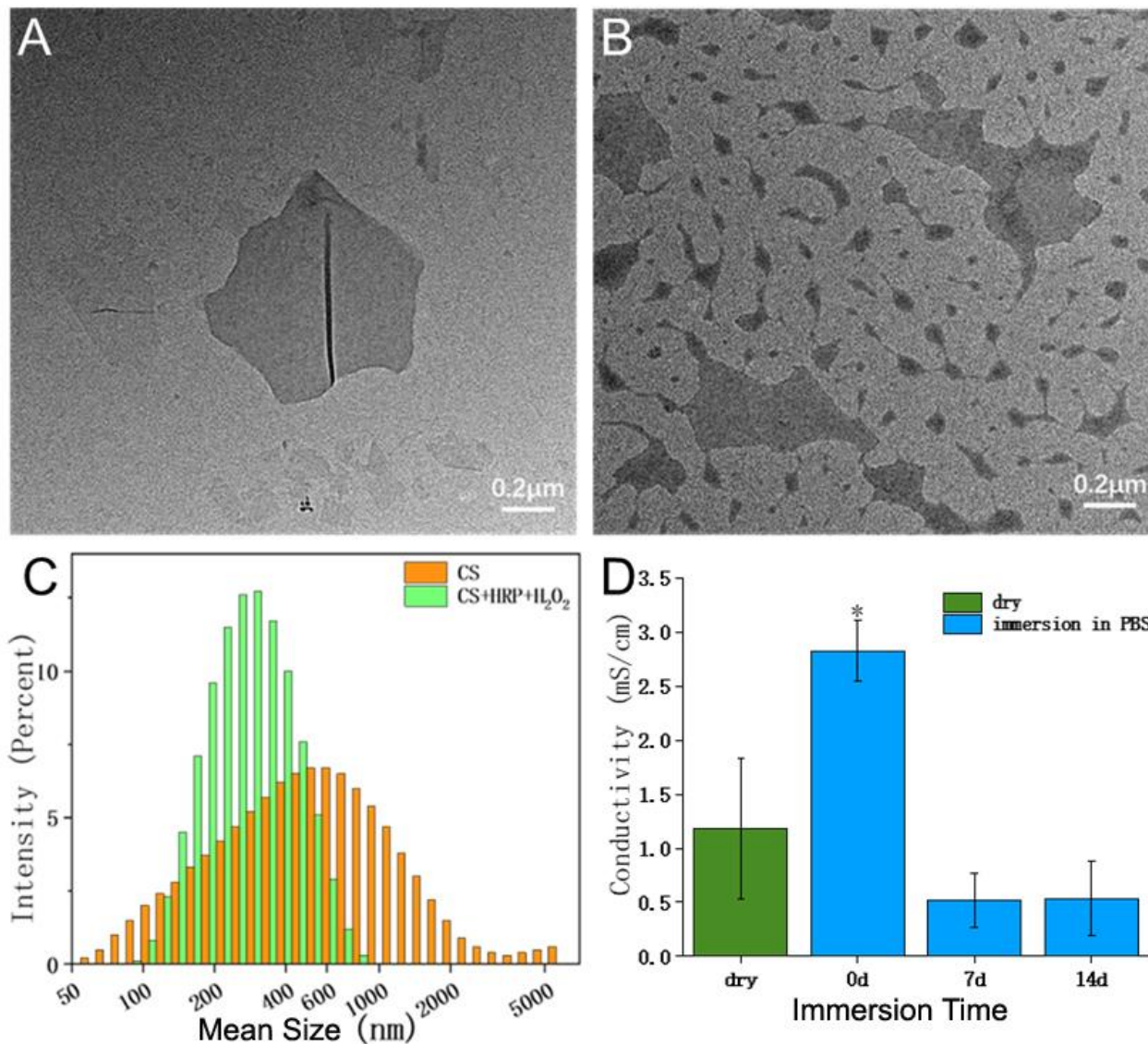
Additional Figure 1 Schematic of preparation of CS-GO scaffold

(A) GO dispersed in CS and electrostatic attraction between the amino groups of CS and carboxyl groups of GO. (B) The amino groups of CS were crosslinked by genipin. CS: Chitosan; CS-GO: graphene oxide-composited chitosan; GO: graphene oxide.



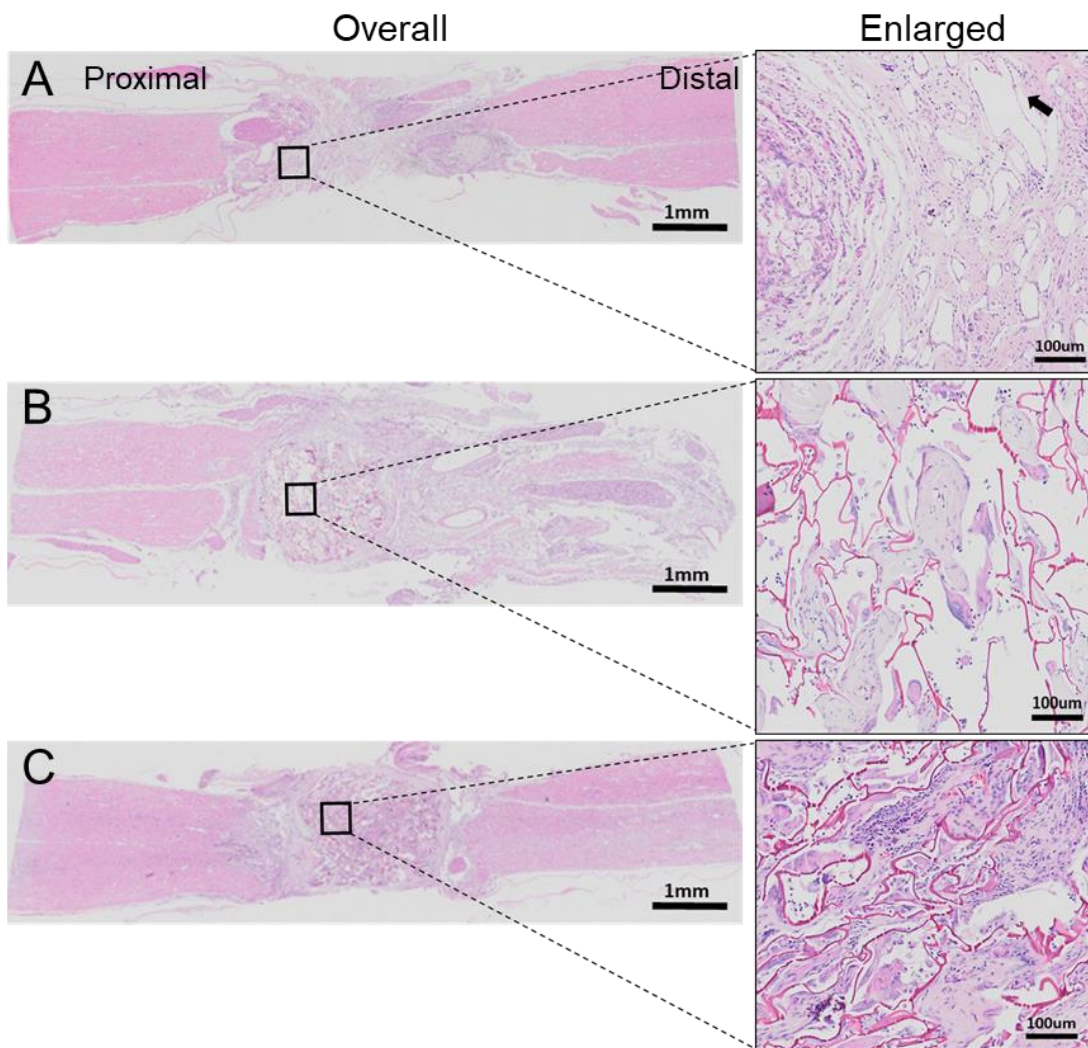
Additional Figure 2 Microstructure and mechanical strength of CS-GO and CS scaffold

(A, B) Scanning electron microscope image of the micropore surface of CS-GO (A) and CS (B) scaffold, and the red arrows pointed to the bulges due to adding GO sheets. Scale bars: 5 μm in A, 10 μm in B. (C) Atomic force microscope image of the surface of CS pores, and 26 nm of the unit of the axis. There were a few of sparse nano-bulges on pore surface of CS scaffold. (D) Elastic modulus of scaffolds after phosphate-buffered saline immersion. CS: Chitosan; CS-GO: graphene oxide-composited chitosan; GO: graphene oxide.



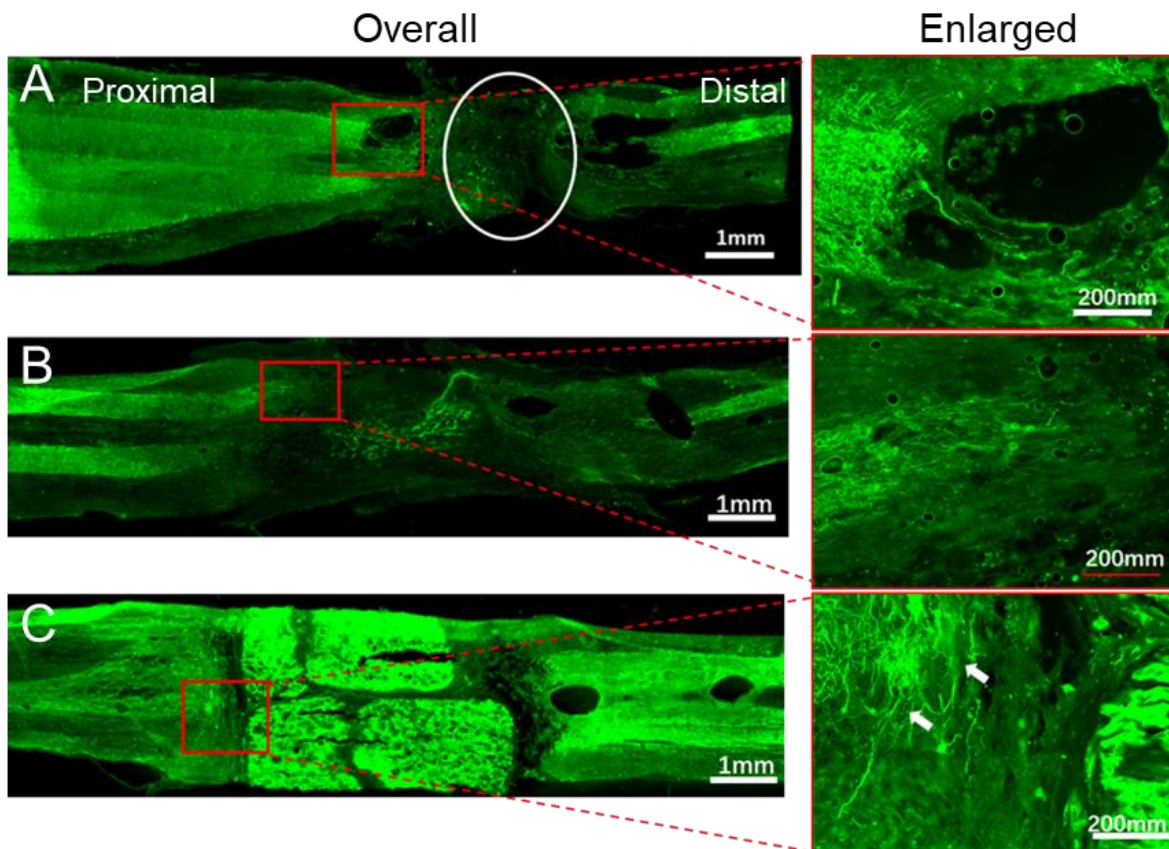
Additional Figure 3 Biodegradation of GO by horseradish peroxidase

(A, B) Transmission electron microscopy images of GO before (A) and after (B) degradation by horseradish peroxidase. Scale bars: 0.2 μm. (C) Size distribution of GO sheets before and after degradation by horseradish peroxidase. (D) Electrical conductivity of CS-GO film before and after immersion in PBS. **P* < 0.05. CS: Chitosan; CS-GO: graphene oxide-composited chitosan; GO: graphene oxide; PBS: phosphate-buffered saline.



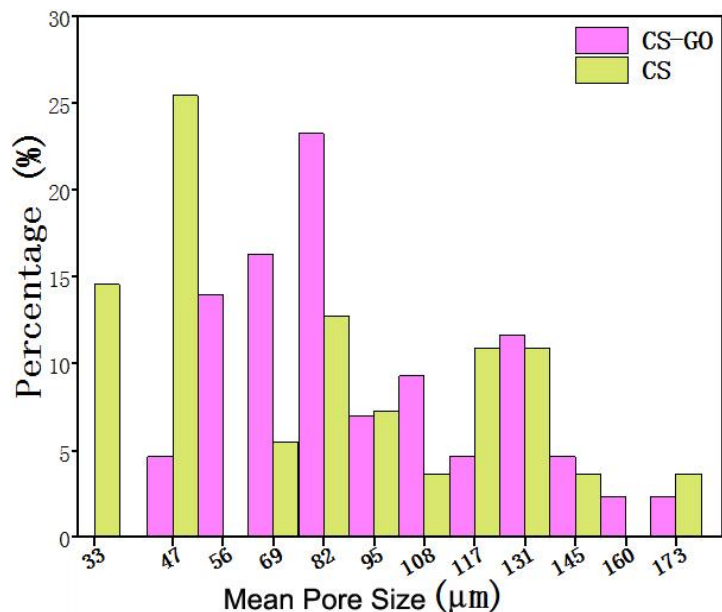
Additional Figure 4 Hematoxylin and eosin staining assessment on the longitudinal sections of the spinal cords of (A) control, (B) CS, (C) CS-GO groups

There are many cavities in control group, and the regenerated tissue grew into the inner structure of CS-GO scaffold, while most of the inner space of CS scaffold kept empty. Arrow indicates cavity. Scale bars: 1 mm (left) and 10 µm (right). CS: Chitosan; CS-GO: graphene oxide-composited chitosan; GO: graphene oxide.



Additional Figure 5 Immunofluorescence (MAP2) staining of the injured site of (A) control, (B) CS, (C) CS-GO groups

There are no regenerated axons in cavities of control group, and only a few of axons in CS group, while there are many regenerated axons in/around CS-GO scaffold. MAP2 (green, stained by Alexa Fluor 488) is a neuronal marker. White circle shows the atrophy and disruption of the spinal cord. White arrows point to the regenerated neurons. Scale bars: 1 mm (left) and 200 mm (right). CS: Chitosan; CS-GO: graphene oxide-composited chitosan; MAP2: microtubule-associated protein-2.



Additional Figure 6 The diameter distributions of the inner micropores of GO-CS and CS scaffolds implanted for 10 weeks, based on the images of hematoxylin and eosin-stained section of their regeneration tissue

CS: Chitosan; CS-GO: graphene oxide-composited chitosan.